Structures 74 (2025) 108642

Contents lists available at ScienceDirect

Structures

journal homepage: www.elsevier.com/locate/structures

# Resilience of hospital structures under seismic loads: A case study informed by the 2023 Maraş earthquake

OZ Ibrahim [1]

*Department of Civil Engineering, Kirsehir Ahi Evran University, Kirsehir 40100, Turkey*

ARTICLE INFO

*Keywords:*
Seismic resilienc
Base isolation systems
Soil-Structure Interaction (SSI)
Nonlinear Time History Analysis (NLTHA)
Hospital buildings

ABSTRACT

This study investigates the seismic performance of a theoretical hospital building designed as a Fixed-Base (FB) structure according to TSC-2018 (Turkish Seismic Code) and evaluates its behavior under three scenarios: Fixed-Base (FB), Soil-Structure Interaction (SSI), and Base-Isolated (SSI+ISO). The study employs Nonlinear Time History Analysis (NLTHA) using scaled acceleration records, including one from the 2023 Maraş earthquake. Structural performance is assessed based on maximum roof displacements, interstory drift ratios (IDR), and isolator displacements. Results show that base isolation systems significantly reduce drift demands and roof displacements, keeping the structure within slight damage limits even under extreme seismic loads. In contrast, SSI effects amplify interstory drift demands, increasing the likelihood of exceeding moderate damage thresholds. The analysis highlights the Maraş Education and Research Hospital, which suffered severe damage and became non-operational during the 2023 Kahramanmaras earthquake. This outcome underscores the limitations of fixed-base designs in regions with soft soil conditions and the necessity of incorporating base isolation systems to improve seismic resilience. The findings emphasize the importance of mandatory adoption of base isolation systems in hospital designs, proper consideration of SSI effects, and the retrofitting of existing hospital buildings to meet modern seismic code requirements (TSC-2018) and prevent similar failures in future seismic events.

## 1. Introduction

On February 6, 2023, a catastrophic earthquake with a magnitude of 7.8 struck Türkiye, severely impacting ten provinces. Official reports indicate that over 50,000 lives were lost, with thousands more suffering injuries ranging from mild to severe. In the aftermath, the functionality and resilience of healthcare facilities in these regions became critically important. Hospitals, as essential infrastructure, must remain operational following seismic events. Consequently, current building codes mandate that hospitals be designed to withstand higher seismic loads to ensure their functionality after an earthquake [1].

In recent years, displacement control studies for structures have emerged as a significant advancement in civil engineering, gaining widespread attention in both academic research and practical applications [2-4]. Forcellini [5] assessed base isolation and SSI interactions through 3D numerical simulations, proposing analytical relationships to predict period elongation and damping increase. Recognizing the inadequacy of relying solely on building importance factors and relative displacement limits for seismic resilience, the Turkish Ministry of Health mandated in 2013 the use of seismic isolators in hospital buildings located in first and second-degree seismic zones with capacities exceeding 100 beds [6]. Furthermore, technical guidelines specified that the foundations supporting these isolators must be designed to remain undamaged during seismic events [7]. However, these requirements apply exclusively to newly constructed hospital facilities. Older hospitals built before the implementation of these regulations were not retrofitted with base isolation systems, leaving them vulnerable during the February 6 earthquakes.

Base isolation systems are primarily designed to mitigate seismic forces transferred from the ground to structures, thereby improving their overall seismic performance. In addition to this primary function, these systems must possess adequate strength to withstand service loads [8-12]. By increasing the vibration period of a structure, base isolation systems effectively reduce spectral accelerations, which in turn lowers the seismic forces acting on the building [13-17]. However, application of base isolator systems faces certain limitations, particularly in soft soil conditions and high-rise structures [18]. Nevertheless, these challenges can be addressed through appropriate engineering practices, as

*E-mail address:* ibrahim.oz@ahievran.edu.tr.
[1] ORCID: https://orcid.org/0000-0003-3152-3675

https://doi.org/10.1016/j.istruc.2025.108642
Received 13 January 2025; Received in revised form 2 March 2025; Accepted 5 March 2025
Available online 10 March 2025

suggested by the same authors. Observations from field studies conducted following the Kahramanmaras Earthquake indicate that isolator systems demonstrated outstanding performance, with hospital structures remaining undamaged and the isolators themselves operating well below their design displacement limits [19].

The growing need for sustainable solutions has further encouraged the development of innovative approaches that combine seismic risk mitigation with ecosystem protection. In this regard, soil-rubber mixtures (SRM) have been introduced as a novel technique to improve the soil beneath foundations, partially dissipating seismic energy within the system. These mixtures, incorporating rubber granules derived from scrap tires, present an environmentally friendly solution while enhancing soil properties for seismic resilience [20]. Abate et al. [21–23] has shown that dynamic soil-structure interaction significantly affects structural response, with studies developing seismic microzonation maps and analyzing non-linear soil behavior. Geological investigations of the Antakya region have shown that the Antakya plain predominantly consists of alluvial soil [24]. When the design of a hospital building in such an environment does not adequately account for soil-structure interaction (SSI) effects, significant discrepancies can emerge between the predicted and actual structural behavior. SSI effects include period elongation caused by flexible soil conditions and foundation movements that display both translational and rotational responses, rather than behaving as infinitely rigid fixed supports [25,26].

Qu et al. [27] conducted post-earthquake field surveys on twelve hospital buildings affected by the February 6 earthquake. Among these structures, five hospitals were equipped with seismic isolation systems, while seven were not. The construction years of the isolated hospitals ranged from 2017 to 2021, whereas the non-isolated hospitals were built between 1968 and 2022. Hospitals utilizing isolation systems were classified as Immediate Occupancy (IO) or Operational (OS), whereas three non-isolated hospitals were deemed unusable. This study underscored the vital role of seismic isolation systems in maintaining the operational functionality of hospital structures during and after major earthquakes. In light of this information, the Antakya Education and Research Hospital, located on soft soil with a shear wave velocity (Vs) of 283 m/s, as reported by the Turkey Disaster and Emergency Management Authority [28], became non-functional following the earthquake. This outcome highlights the vulnerability of structures constructed without base isolation systems, particularly in regions with soft soil conditions [27].

During the recent Maras earthquake, hospital buildings in certain regions sustained damage. Field observations indicate that the affected buildings lacked displacement control measures such as base isolation systems Qu et al. [27]. However, limited analytical studies have been conducted on this subject. This study specifically considers Soil-Structure Interaction (SSI) effects, which are not mandatory in design calculations according to current regulations. Although hospitals are designed as Fixed-Base (FB) structures based on updated codes, their collapse during such a major earthquake suggests a need for further regulatory improvements. Moreover, studies that simultaneously consider both base isolation and SSI effects remain quite limited in the literature.

This study aims to assess the seismic vulnerability of a theoretical three-dimensional hospital building designed in compliance with TSC-2018 DBE by analyzing its structural behavior under three distinct scenarios: fixed-base, soil-structure interaction (SSI), and base-isolated systems. The evaluation of seismic performance focuses on key damage indicators, including maximum roof displacement demand, maximum inter-story drift ratios, and maximum isolator displacements. Three-dimensional dynamic analyses were conducted to simulate structural behavior under each scenario, incorporating both east-west and north-south components of seismic acceleration records simultaneously to achieve a realistic representation of seismic response. A total of eight ground motion records were employed, seven sourced from the Pacific Earthquake Engineering Research Center (PEER) and one from the nearest seismic station (Station 3124). Nonlinear soil behaviors, such as liquefaction, were intentionally excluded from the study's scope. Instead, the surrounding soil medium was modeled using linear spring elements, in accordance with NIST-2012 guidelines.

## 2. Materials and methods

### 2.1. Design and modelling of the hospital building

As the subject of this study is a theoretical hospital building, the floor plan was carefully designed and developed specifically for this research. This theoretical structure was conceptualized as a replacement for the severely damaged Hatay Education and Research Hospital, which suffered extensive structural damage during the February 6, 2023 earthquake. While not directly replicating the original architectural layout, the design reflects structural characteristics commonly observed in hospital buildings, such as arc-shaped elements, which are frequently encountered in real-world hospital plans. These elements were intentionally incorporated to better simulate the structural behavior typically observed in such designs under seismic loading. Furthermore, the detailing of shear walls and the preliminary dimensions of reinforced concrete columns and beams were determined during the structural design phase, adhering to the standards and guidelines outlined in TSC-2018. This approach ensures that the theoretical model remains both analytically robust and representative of real-world hospital structures without relying on predefined templates or existing building designs.

The story height was uniformly set at 4.5 m across all floors. A three-dimensional view of the hospital building is presented in Fig. 1. Non-structural walls and slabs were not modeled explicitly; instead, their effects were represented as equivalent loads applied on the relevant beams. The dead loads considered for different slabs range between 2.5 kN/m$^2$ and 3.5 kN/m$^2$, while live loads vary between 2.0 kN/m$^2$ and 5.0 kN/m$^2$.

The hospital building was designed specifically for the location of the Hatay Antakya Education and Research Hospital. During the design process, the design spectrum for this location was derived from the AFAD Turkey Earthquake Hazard Maps Interactive Web Application. The geographical coordinates used were 36.224° E and 36.270° N. To determine the seismic design forces, the demand spectrum obtained from the application was reduced using the seismic load reduction coefficient (R) to generate the reduced design spectrum. Additionally, the Ra coefficient was calculated separately for two regions by comparing the spectrum's corner period using Eq. (1) and Eq. (2).

$$Ra(T) = \frac{R}{I};\ \mathrm{T} > \mathrm{TB} \tag{1}$$

$$Ra(T) = D + \left(\frac{R}{I} - D\right)\frac{T}{TB} \tag{2}$$

In determining the R value, the parameters D (overstrength factor) and I (structural behavior factor), as defined in TSC-2018, were also considered. For the hospital building analyzed in this study, the values were selected as R = 6, I = 1.5, and D = 2.5. The vibration periods corresponding to the x and y directions, as well as the seismic forces acting on the building, were calculated and appropriately distributed across the stories. Although TSC-2018 specifies different R and D coefficients for base-isolated buildings, the same building initially designed with a fixed-base support system was analyzed with a base isolation system to ensure a consistent evaluation framework. Furthermore, according to TSC-2018, for buildings classified under Seismic Design Class 1a that are to be retrofitted with seismic isolation, the advanced performance objective is defined as Limited Damage (LD) at the Design Basis Earthquake (DBE) ground motion level [7]. In this study, the structure was analyzed with R = 1.2 and D = 1.2, and the required isolator displacements were determined accordingly, forming the basis for isolator design.

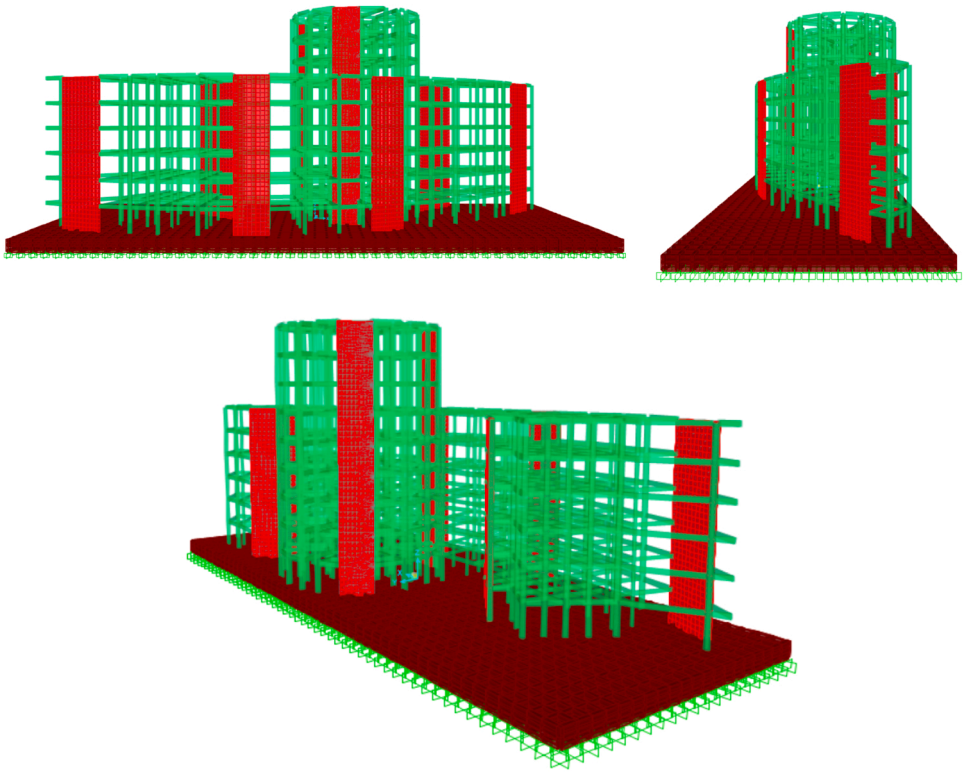

**Fig. 1.** 3D View of the Analyzed Hospital Building.

In TSC-2018, the performance objectives vary depending on the design approach applied. For the seismically isolated building, the advanced performance objective is defined as Immediate Occupancy (IO), whereas for the fixed-base building, it is defined as Controlled Damage (CD). Therefore, while the intended purpose of the structure remains consistent, the performance objectives differ based on the selected design methodology. The Design Basis Earthquake (DBE) and Maximum Considered Earthquake (MCE) spectra used in the design process are illustrated in Fig. 2.

The hospital building design incorporated circular cross-sections for the columns, with dimensions selected as R60, R80, and R100, while beam dimensions were determined as 30 × 60 cm and 30 × 70 cm. Column reinforcement ratios ranged between 1.08 % and 3.01 %, and the shear wall thickness was designed as 60 cm, with a longitudinal reinforcement ratio of 0.2 %. The structure spans approximately 90 m in length along the X-direction and varies in width from 4 m to 29 m in the Y-direction, with a shear wall-to-floor area ratio of about 2.1 %. Design standards such as TSC-2018 and Eurocode 2005 [29] recommend using reduced moments of inertia (Ieff) for reinforced concrete (RC) elements during both the design and evaluation stages. Accordingly, the effective stiffness values were defined as 0.35I for beams, 0.7I for columns, and 0.5I for shear walls, following the guidelines in TSC-2018. Structural

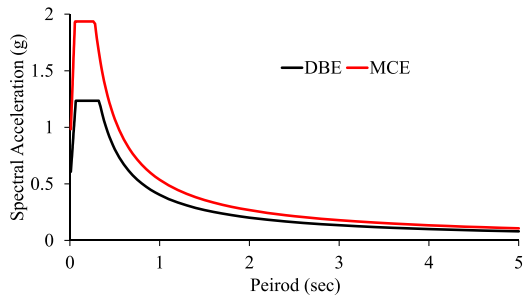


**Fig. 2.** Design response spectra of the subjected structure.

analysis results indicated a fixed-base period of 0.822 seconds in the X-direction and 0.608 seconds in the Y-direction. Effective inter-story drifts (δi), derived from seismic loads based on the reduced spectrum and calculated by incorporating 30 % of the seismic force from the orthogonal direction (Ex + 0.3Ey for the X-direction), were ensured to remain within the effective relative displacement limits specified by the regulations.

Three-dimensional structural models were developed using SAP2000 version 23.3.1, a widely recognized structural analysis software for dynamic assessments. To accurately capture the nonlinear behavior of frame structural members, lumped fiber-hinge elements were employed, where hinges were directly defined based on material nonlinearity. Each hinge was modeled using fiber elements, with stiffness derived directly from the nonlinear characteristics of the material. According to Carvalho et al. [30], a single hinge at each end of a member is sufficient to simulate biaxial bending, with the hinge length set to 0.5 times the section height. For circular columns, an additional length of 10 % of the clear column height was added to half the column diameter, and plastic hinge lengths were calculated as ($L_p$= 0.5d+0.1 L). For shear walls, nonlinear layered shell elements were used with a maximum of 10 cm area mesh to represent their behavior effectively. The compressive strength of concrete was assumed to be 40 MPa, while the yield strength of both longitudinal and transverse reinforcements was taken as 420 MPa. The calculations also accounted for the post-yield strengthening behavior of the reinforcement.

The beam–column joint rigid offset modeling approach followed the methodology proposed by Abdel Raheem et al. [31];. In this method, beam and column frame members were connected through rigid offsets, with dimensions corresponding to the depth of the framing members. Additionally, the rigid diaphragm effects of the slabs were incorporated to ensure in-plane rigidity across floor levels. The stiffness contribution of infill walls was neglected, as these walls typically detach from reinforced concrete (RC) members during early damage stages. Consequently, infill walls were not physically modeled as part of the slabs in the structural analysis. Both P-Δ effects and rigid-diaphragm behavior

were included in the modeling scope.

For the nonlinear time-history (NLTH) analysis, SAP2000 was used. The Newmark-beta method [32] was applied, with the γ (gamma) and β (beta) coefficients set to 0.5 and 0.25, respectively, ensuring unconditional stability. Rayleigh damping was used to define the damping properties, with a 5 % damping ratio assumed. The mass and stiffness proportional damping coefficients were calculated based on varying period values and integrated into the viscous damping formulation, ensuring a mass participation ratio exceeding 95 %. A convergence tolerance of $10^{-4}$ was chosen for the nonlinear time-history analyses, ensuring numerical stability and accuracy.

### 2.2. Soil-structure model

The substructure method was employed to represent soil-structure interaction (SSI) effects. A critical step in this approach involves determining the foundation's impedance functions, which significantly influence the seismic behavior of the structure, including its vibration period [33]. These effects are often referred to as inertial effects [34]. The substructure approach is generally categorized into lumped models and cone models. In this study, a lumped parameter model was chosen to simulate the foundation's stiffness and damping using lumped springs. However, it is worth noting that most lumped parameter models assume ideal conditions, such as shallow foundations on homogeneous elastic half-spaces. Previous research, including studies by NIST [34]; Pais, Kausel [35], has proposed several lumped impedance functions. In this approach, the superstructure can be modeled as either a single-degree-of-freedom (SDOF) or a multi-degree-of-freedom (MDOF) system [34,36]. The soil-foundation system was modeled using groups of linear-elastic springs and dashpots, which were connected to the superstructure through foundation elements [34]. The stiffness and damping properties of these springs and dashpots were calculated using widely accepted NIST [34] equations, frequently referenced in seismic research [34,36,37]. The shear modulus (G) of the analyzed soil conditions was derived using Eq. (3), where $V_s$ represents the shear wave velocity, G is the shear modulus, and $\rho_s$ refers to the soil mass density. The mechanical properties of the soils analyzed, including mass densities and Poisson's ratios, are presented in Table 2.

$$Vs = \sqrt{\frac{G}{\rho s}} \tag{3}$$

The springs and dashpots were initially calculated assuming surface foundation conditions (i.e., foundation embedment = 0). Stiffness modifiers were then applied to account for embedment effects, with these modifiers determined based on the vibration periods of the structure in the Tx and Ty directions. Similarly, radiation damping ratios were calculated considering the soil and structural properties. The surface springs and dashpots were adjusted using this stiffness and damping modifiers, resulting in the final stiffness ($k_z^i$) and damping ($c_z^i$) properties of the foundation-soil system. Since soil behavior is not perfectly linear along the vertical axis, the stiffness ($k_z^i$) values were increased along the foundation edges, while damping ($c_z^i$) values were decreased. An edge length ratio of 0.4 was assumed, consistent with the typical range of 0.3–0.5. The foundation elements were modeled similarly to methodologies adopted in previous studies [34,38]. Elastic frame members were attached to the bottom ends of the ground story columns to simulate the foundation's response under vertical, horizontal, and moment loading, without incorporating hinges. Due to their inherent characteristics, spring elements respond exclusively to loads acting parallel to their axis [34], and perpendicular loads do not influence their behavior. As a result, the stiffness and damping properties were calculated independently for each direction and assigned as uniaxial link elements to the foundation of the superstructure, ensuring an accurate representation of soil-structure interaction across the defined area ($d_A$). A schematic diagram illustrating the connection between link-foundation and superstructure elements is provided in Fig. 3. The used substructure method offers a simpler alternative to the direct method, where the nonlinear behavior of the soil is explicitly modeled. Additionally, the Nonlinear Time History Analysis (NLTHA) results can be obtained more efficiently due to the reduced number of analyzed elements. A verification study comparing the substructure method with the linear elastic direct method revealed that, despite minor differences in results for linear soil behavior, the substructure method remains sufficiently accurate and applicable [39].

The natural vibration periods derived from the analysis, which included SSI effects, were consistently longer than those obtained from the fixed-base approach across all evaluated structures. This observation highlights the significant impact of SSI on the dynamic behavior of structures. The elongation of the natural period generally reduces the spectral acceleration experienced by the structure, potentially lowering seismic demand. However, this effect is not uniform and is influenced by factors such as foundation stiffness and soil properties. Therefore, SSI effects must be carefully considered in the seismic design and evaluation of structures.

### 2.3. Base isolated model

In this study, a theoretical hospital building with a total of 116 designed columns was retrofitted with seismic isolation systems in accordance with regulatory requirements. A Lead Rubber Isolator (LRB) was installed beneath each column in the structure. The connections of the shear walls in the model were detached from the foundation and linked to a rigid isolation slab, which was assumed to remain undamaged during an earthquake [40,41]. The details of the isolators designed in this study are presented in Table 1, while the displacement-force graphs for the designed isolator elements in the x and y directions are shown in Fig. 4.

The fixed-base, SSI, and base-isolated periods of the reinforced concrete hospital building with a fixed support design, examined within the scope of this study, are presented in Table 2 for the x and y directions.

### 2.4. Selection of ground motions

In this study, a total of eight acceleration records were utilized, including one record from the 7.8 Mw Kahramanmaras earthquake and seven records sourced from the PEER [42] Strong Ground Motion Database. During the selection of these acceleration records, particular attention was given to ensuring that the shear wave velocities ($V_{s30}$) of the recording stations closely matched the shear wave velocity of $V_{s30}$ = 283 m/s of the station 3124, representing the soil conditions of the analyzed building. The station information, moment magnitudes ($M_w$), and other relevant details of the acceleration records used are presented in Table 3. A comparison of the spectral accelerations of these records with both the Maximum Considered Earthquake (MCE) level and the Kahramanmaras earthquake record is presented in Fig. 5. During this comparison, it was observed that the spectral accelerations of the selected records were significantly lower than those of the Kahramanmaras earthquake. To address this discrepancy, a simple scaling method was applied, increasing the average spectral acceleration of the other seven records by constant scaling factors to match the spectral acceleration of the Kahramanmaras earthquake. The scaled acceleration records and their comparison with the Kahramanmaras earthquake record and MCE levels are shown in Fig. 6, and the applied scale factors to each record are provided in Table 4.

During the scaling of acceleration records, the Kahramanmaras earthquake was directly chosen as the target spectrum instead of the Maximum Considered Earthquake (MCE) level. This decision was made because the spectral acceleration of the Kahramanmaras earthquake exceeds the spectral acceleration derived from the site-specific seismic hazard map in certain frequency ranges. To account for the worst-case

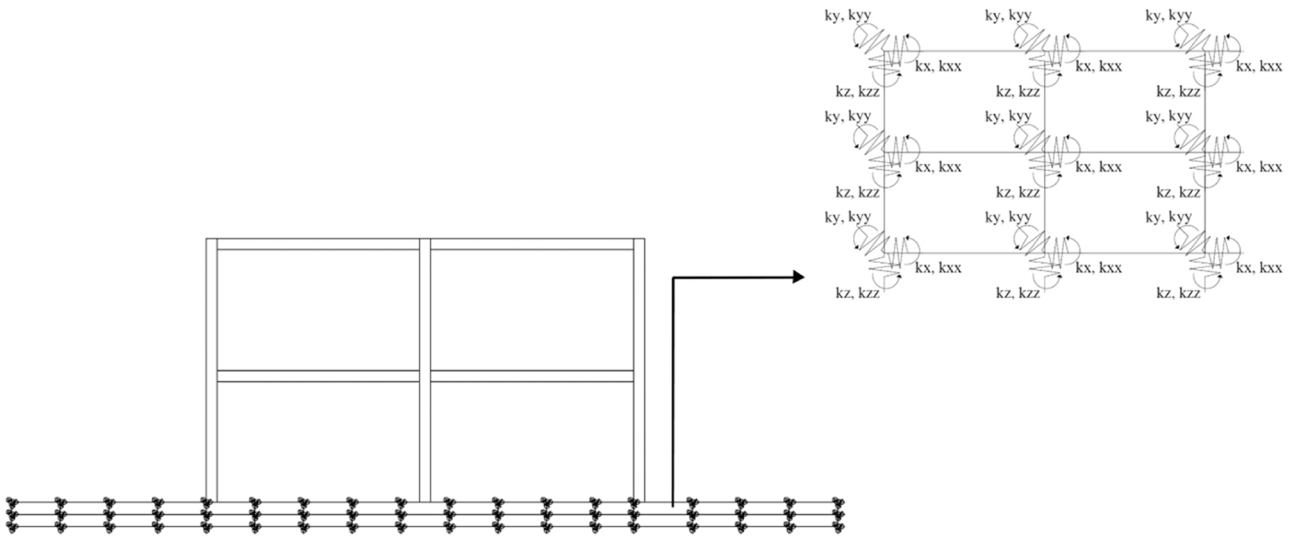


**Fig. 3.** Schematic illustration of connection of link-foundation and superstructure elements.

**Table 1**
Design parameters of the used LRB type isolators.

| $k_v$ (kN/m) | $k_e$ (kN/m) | $k_2$ (kN/m) | $F_y$ (kN) | $k_2/k_1$ | $\xi_{eff}$ | Dmax (m) |
|---|---|---|---|---|---|---|
| 69282.65 | 557.0508 | 2129.607 | 237.5829 | 0.406795 | 0.25 | 0.6 |

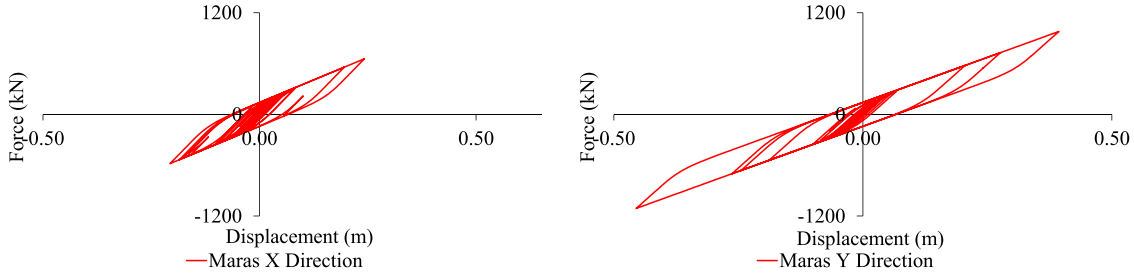


**Fig. 4.** Force-displacement relationship of isolators under Maras earthquake.

**Table 2**
Vibration periods of considered cases.

| | Fixed Base | SSI | SSI with base isolation |
|---|---|---|---|
| **Tx (sec)** | 0.822 | 1.011 | 3.302 |
| **Ty (sec)** | 0.608 | 0.759 | 3.252 |

scenario, a scaling method was applied, ensuring that the average spectral acceleration of the selected records closely matched that of the Kahramanmaras earthquake. This approach aimed to more accurately represent the intensity and frequency characteristics observed during the Kahramanmaras earthquake, providing a realistic assessment of the seismic demands on the analyzed hospital structure.

## 3. Results and discussion

The displacement results from the three-dimensional Nonlinear Time History (NLTH) analyses of the hospital building, designed as a Fixed Base (FB) structure in accordance with TSC-2018, were evaluated across three scenarios: Fixed Base (FB), Soil-Structure Interaction (SSI), and SSI with isolators. The assessment of the structural damage state was conducted using three critical parameters: maximum isolator displacements [2], inter-story drift limits [43], and roof displacement values [2]. These parameters provided insight into the building's behavior and performance under seismic loading conditions. The observed damage

**Table 3**
The properties of ground motions considered in this study.

| Record Sequence Number | Earthquake Name | Year | Station Name | Magnitude | Vs30 (m/sec) | PGA |
|---|---|---|---|---|---|---|
| 752 | Loma Prieta | 1989 | Capitola | 6.93 | 288.62 | 2.31 |
| 949 | Northridge−01 | 1994 | Arleta - Nordhoff Fire Sta | 6.69 | 297.71 | 1.31 |
| 959 | Northridge−01 | 1994 | Canoga Park - Topanga Can | 6.69 | 267.49 | 1.77 |
| 1044 | Northridge−01 | 1994 | Newhall - Fire Sta | 6.69 | 269.14 | 3.24 |
| 1048 | Northridge−01 | 1994 | Northridge - 17645 Saticoy St | 6.69 | 280.86 | 1.93 |
| 1063 | Northridge−01 | 1994 | Rinaldi Receiving Sta | 6.69 | 282.25 | 2.67 |
| 1120 | Kobe_ Japan | 1995 | Takatori | 6.90 | 256.00 | 2.91 |

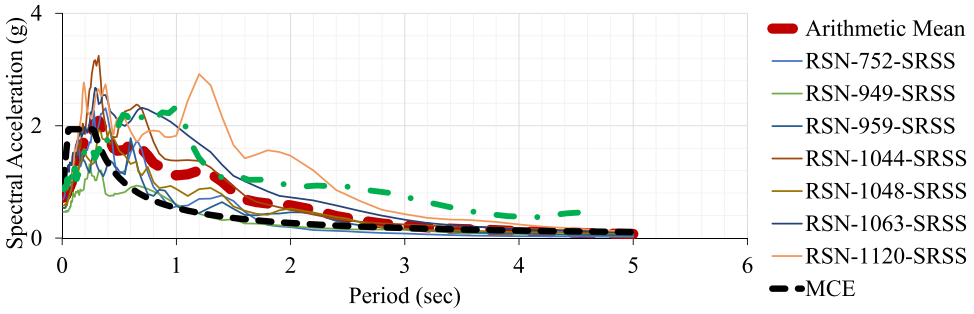


**Fig. 5.** Unscaled spectra and MCE.

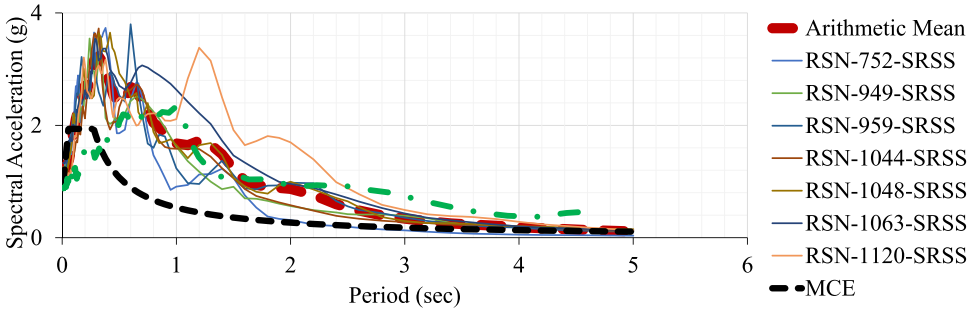


**Fig. 6.** Scaled spectra and MCE.

**Table 4**
Scale factors of considered earthquakes.

| Earthquake | Scale Factor |
|---|---|
| RSN−752-SRSS | 1.614 |
| RSN−949-SRSS | 2.697 |
| RSN−959-SRSS | 2.134 |
| RSN−1044-SRSS | 1.147 |
| RSN−1048-SRSS | 1.888 |
| RSN−1063-SRSS | 1.322 |
| RSN−1120-SRSS | 1.158 |

conditions and their corresponding damage limits are presented in Table 5, serving as a benchmark for evaluating the effectiveness of each structural configuration in mitigating seismic damage.

### 3.1. Comparison of IDRs

In this study, since acceleration records exceeding the MCE level were used, an alternative statistical method was applied instead of relying solely on maximum inter-story drift ratios. For this approach, the inter-story drifts ($u_i$-$u_{i-1}$) were calculated for each time step (dt) recorded from the NLTH analyses and then normalized by the story heights. The absolute values of the resulting inter-story drifts were taken and ranked in ascending order for each acceleration record. This process allowed for the determination of inter-story drift values corresponding to exceedance probabilities of (PoE) 10 % and 2 %. The average inter-story drift values for each earthquake scenario are presented in Fig. 7, and the IDR limits of 0.3 %, 0.6 %, 1.5 %, and 2 % are marked on these graphs.

**Table 5**
Damage states and corresponding threshold values.

| | Damage Measure / Threshold | | |
|---|---|---|---|
| **Damage State** | **Max Isolator Displacement** | **Inter-story Drift Ratio** | **Roof Drift Ratio** |
| Slight | 0.2 $D_{max}$ | 0.30 % | 0.10 % |
| Moderate | 0.4 $D_{max}$ | 0.60 % | 0.50 % |
| Extensive | 0.8 $D_{max}$ | 1.50 % | 1.00 % |
| Collapse | 1.2 $D_{max}$ | 2.00 % | 2.00 % |

The Fig. 7. displays the mean interstory drift ratios (IDRs) for exceedance probabilities of 2 % and 10 % in both X and Y directions, with the damage measure limits of 0.3 %, 0.6 %, 1.5 %, and 2 % indicated by dashed lines. Across all scenarios (FB, SSI, and SSI+ISO), the base isolated system (red line) consistently results in lower IDRs, remaining well below critical safety limits. The FB (blue line) and SSI (green line) scenarios show relatively higher IDRs, with some points nearing or exceeding the 1.5 % and 2 % thresholds, particularly in the PoE 2 % exceedance graphs. These results highlight the effectiveness of base isolation systems in reducing seismic demands on the structure. This situation highlights the necessity of retrofitting the Hatay Training and Research Hospital, which became unusable during the Kahramanmaras earthquake (reported as collapse prevention by Qu et. al, 2023), in compliance with the updated regulations [1] and by implementing seismic isolation systems.

For hospital buildings, immediate occupancy or operational continuity conditions are required after an earthquake ([7], TSC 2018). As observed in the graphs, the structure remains within the slight damage phase for 10 % PoE IDR and 2 % PoE IDR, which correspond to DBE (Design Basis Earthquake) and MCE (Maximum Considered Earthquake) levels. However, the same observation does not apply to both Fixed-Base (FB) and Soil-Structure Interaction (SSI) scenarios. For 2 % PoE (MCE), the hospital building experiences moderate damage in both cases, in both directions. Nevertheless, a hospital building designed in accordance with seismic codes demonstrates moderate damage during such an earthquake while still ensuring life safety. When analyzing the green graph (SSI scenario), it becomes clear that Soil-Structure Interaction (SSI) plays a significant role in the seismic response of the structure. It also increases the exceedance probabilities of IDRs corresponding to DBE (Design Basis Earthquake) and MCE (Maximum Considered Earthquake) levels.

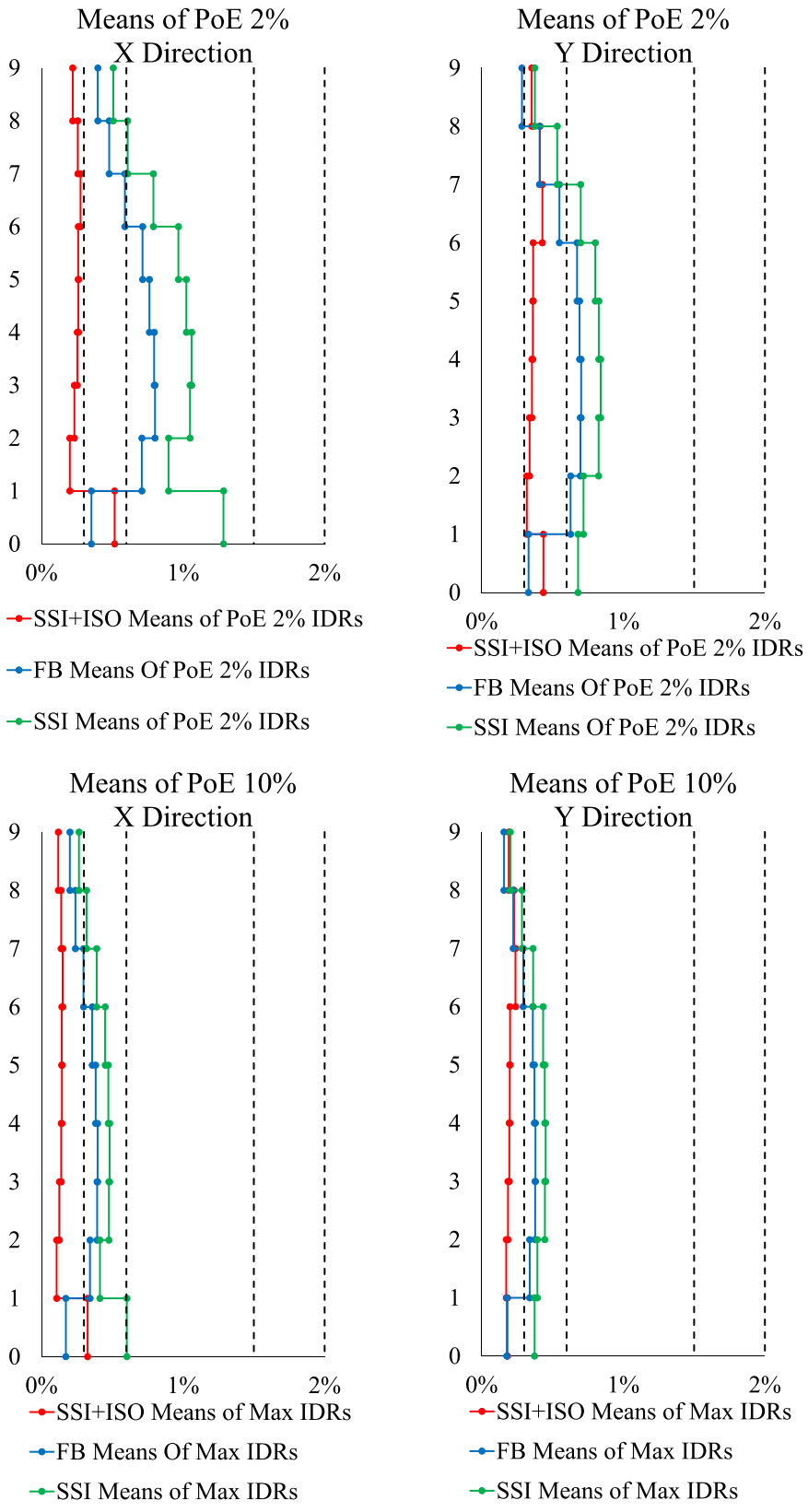


**Fig. 7.** IDR of corresponding 10 % and %2 probability of exceedance.

### 3.2. Base isolator displacements

Fig. 8 illustrates maximum isolator displacement for various earthquake records. Damage states are categorized by red dashed lines into Slight ($< 0.2\ D_{max}$), Moderate ($0.2D_{max} < D < 0.4D_{max}$), Extensive ($0.4D_{max} < D < 0.8D_{max}$), and Collapse ($> 1.2\ D_{max}$) thresholds. All the isolator displacements fall within the Slight and Moderate damage ranges, with none reaching the Extensive or Collapse damage

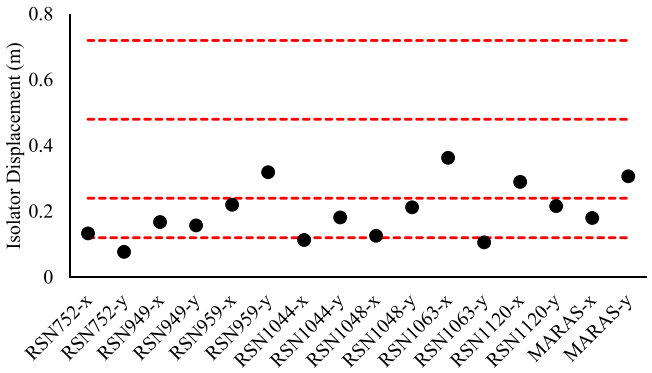


**Fig. 8.** Maximum isolator displacements and damage thresholds.

thresholds. This indicates that the isolators effectively dissipated seismic energy across all analyzed scenarios. Overall, the results demonstrate that the isolators performed as intended, preventing significant damage and ensuring structural safety under strong seismic demands.

The fragility curves shown in the Figs. 9 and 10 are developed using a lognormal cumulative distribution function (CDF) to estimate the probability of exceeding specific damage states based on the roof drift ratio as the engineering demand parameter (EDP) [40]. The fragility function is derived from Eq. (4), and the probabilities of exceedance for isolator displacements are presented in Fig. 9. Fig. 9 presents fragility curves for base isolators derived using Eq. (4), showing the probability of exceeding slight, moderate, and extensive damage states based on maximum isolator displacement. Slight damage occurs at low displacements (~0.1 m), moderate damage between 0.15–0.2 m, and extensive damage beyond 0.3 m. The results indicate that base isolators can accommodate significant displacement before reaching severe damage. Notably, in none of the cases did the isolators experience extensive damage, demonstrating their effectiveness in protecting structures.

$$P(D > s|\ IM) = \Phi\left(\frac{(\ln(IM) - \ln(\mu)}{\sigma}\right) \quad (4)$$

where:P is the probability of the structural damage (D) exceeding damage state;Φ is the standard normal cumulative distribution function; IM is the selected intensity measure value;σ is the standard normal deviation andμ is the mean of the lognormal seismic intensity measure.

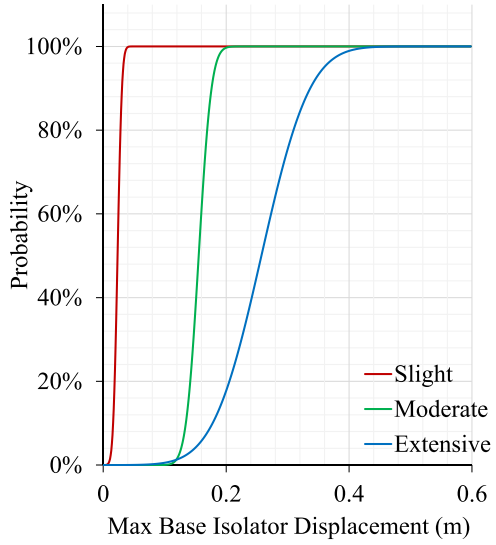


**Fig. 9.** Fragility curves for base isolators.

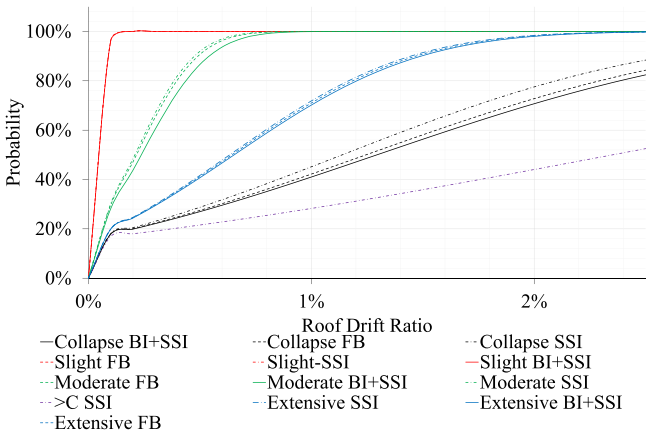


**Fig. 10.** Fragility curves for FB, SSI, and BI+SSI systems.

### 3.3. Comparison of Roof Drifts

Fig. 10 displays fragility curves in terms of roof drift ratio for structures with a fixed base (FB), soil-structure interaction (SSI), and base isolation (BI+SSI). Collapse probabilities are higher for SSI cases, while FB and BI+SSI systems exhibit lower probabilities of exceedance (PoEs), indicating better seismic performance. Base isolation effectively reduces collapse risk. As seen in Fig. 10, the only case where the collapse state is exceeded occurs in the soil-structure interaction (SSI) model.

In Fig. 11, the roof displacement-time series of the building with the isolator system is presented. By excluding the isolator displacements, the maximum roof story drifts were compared for the Fixed Base (FB) and Soil-Structure Interaction (SSI) scenarios within the damage limits examined in this study.

Fig. 12 illustrates the Maximum Roof Drift Ratios (MRDR) for three structural scenarios: Fixed-Base (FB, diamonds), Soil-Structure Interaction (SSI, crosses), and Base-Isolated (triangles). The horizontal dotted lines represent damage thresholds corresponding to no damage (0.0 %–0.1 %), slight damage (0.1 %–0.5 %), moderate damage (0.5 %–1.0 %), extensive damage (1.0 %–2.0 %), and collapse (>2.0 %). In the Base-Isolated scenario, MRDR values consistently remain below the 1.0 % slight damage threshold, demonstrating the effectiveness of seismic isolation systems in controlling structural drifts and reducing damage potential. In contrast, the SSI scenario exhibits higher variability, with several points surpassing the 1.0 % moderate damage threshold and even approaching the 2.0 % extensive damage limit. This indicates that soil-structure interaction effects can amplify drift demands, posing a risk for more significant damage under certain seismic conditions. The Fixed-Base scenario shows a relatively stable response compared to the SSI case but still includes instances where drifts exceed the moderate damage threshold. Overall, the results highlight the superiority of base isolation systems in maintaining structural safety and minimizing drift demands. Additionally, the findings underscore the importance of accounting for soil-structure interaction effects in seismic design, particularly for critical facilities such as hospitals, to ensure both structural integrity and post-earthquake operability.

## 4. Conclusions

In this study, the seismic performance of a hospital structure was evaluated under three different scenarios: Fixed-Base (FB), Soil-Structure Interaction (SSI), and Base-Isolated (SSI+ISO). Nonlinear Time History Analysis (NLTHA) was conducted using scaled ground motion records, including one from the 2023 Kahramanmaraş Earthquake. The seismic response of the structure was assessed based on key engineering demand parameters, such as maximum roof displacements, interstory drift ratios (IDRs), and isolator displacements. The findings

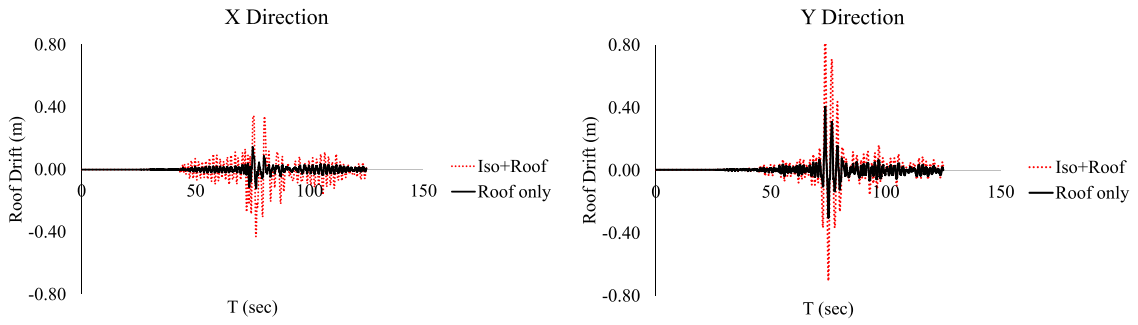


**Fig. 11.** Roof displacements of the examined building with and without isolator displacements under Maras earthquake.

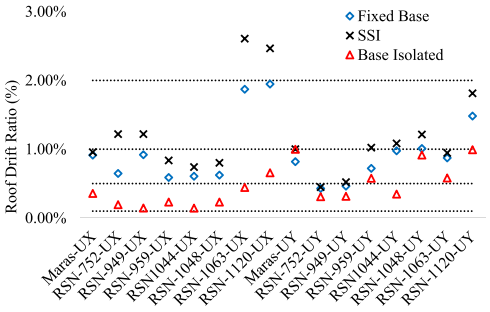


**Fig. 12.** Maximum roof drifts and damage thresholds.

obtained from the analysis are summarized below.

The results confirm that base isolation is highly effective in limiting seismic damage. Under all earthquake scenarios, the base-isolated structure exhibited significantly lower interstory drift ratios and roof displacements, remaining within the slight damage range. This demonstrates that base isolation ensures not only the structural integrity of hospital buildings but also their continued functionality following major earthquakes.

The influence of soil-structure interaction (SSI) on structural response was also evident. While SSI effects resulted in an elongation of the building's vibration period, they also led to significantly higher interstory and roof drift demands compared to the fixed-base (FB) scenario. As seen in Fig. 12, the SSI model exceeded the collapse threshold for maximum roof drift, whereas the FB model did not reach this limit, highlighting the detrimental impact of SSI effects in soft soil conditions. On the other hand, the base-isolated (BI) structure consistently remained within the limited damage or operational performance level, even under the most severe seismic demands, proving its superior effectiveness in maintaining structural integrity and post-earthquake functionality.

A comparison of fixed-base and base-isolated hospital structures reveals that the fixed-base hospital failed to meet immediate occupancy performance objectives under strong seismic loading. Moderate damage was observed in both the FB and SSI models, whereas the base-isolated system maintained a slight damage state, proving its superior seismic resilience.

The performance of the base isolation system was further validated through isolator displacement analysis. Across all earthquake records, isolator displacements remained within the moderate damage range, confirming that the seismic isolation system effectively dissipated seismic energy without exceeding critical displacement limits. This ensures that hospitals equipped with base isolation can remain operational after major seismic events.

Lastly, the fragility analysis confirmed that the probability of exceeding collapse thresholds is significantly higher in SSI cases compared to FB and base-isolated structures. This underscores the importance of incorporating soil-structure interaction effects in seismic performance evaluations, particularly for critical facilities such as hospitals. The findings emphasize that base isolation is not only a structural safety measure but also a key factor in maintaining healthcare service continuity following a major earthquake.

## CRediT authorship contribution statement

**OZ Ibrahim:** Software, Methodology, Investigation, Formal analysis.

## References

[1] Ministry of Environment and Urbanization. 2018. Turkey building earthquake code. [In Turkish.] Ankara, Turkey: Earthquake Code Preparation Committee.
[2] Şen F, Sunca F, Altunişik AC. Seismic performance assessment of a base-isolated hospital building subjected to February 6, 2023, Kahramanmaraş, Türkiye earthquakes (Mw 7.7 Pazarcık and Mw 7.6 Elbistan) and seismic fragility analysis considering different construction stages. Soil Dyn Earthq Eng 2024;185:108876. https://doi.org/10.1016/j.soildyn.2024.108876.
[3] Matsagar VA, Jangid RS. Impact response of torsionally coupled base-isolated structures. J Vib Control 2010;16(11):1623–49. https://doi.org/10.1177/1077546309103271.
[4] Pisal AY, Jangid RS. Dynamic response of structure with tuned mass friction damper. Int J Adv Struct Eng 2016;8(4):363–77. https://doi.org/10.1007/s40091-016-0136-7.
[5] Forcellini D. The assessment of the interaction between base isolation (BI) technique and soil structure interaction (SSI) effects with 3D numerical simulations. Structures 2022;45:1452–60. https://doi.org/10.1016/j.istruc.2022.09.080.
[6] Erdik, M., Tuzun, C., & Ulker, O. (2015). Evaluation of seismic isolation applications of health care facilities in Turkey. In Proceedings of the 14th World Conference on Seismic Isolation, Energy Dissipation and Active Vibration Control of Structures, San Diego (CA), USA.
[7] Erdik M, Ülker € O, S¸adan B, Tüzün C. Seismic isolation code developments and significant applications in Turkey. Soil Dyn Earthq Eng 2018;115:413–37. https://doi.org/10.1016/j.soildyn.2018.09.009.
[8] Ozer E, Inel M, Cayci BT. Seismic performance comparison of fixed and base-isolated models. Iran J Sci Technol, Trans Civ Eng 2023;47(2):1007–23. https://doi.org/10.1007/s40996-022-00936-4.
[9] Ceccoli C, Mazzotti C, Savoia M. Non-linear seismic analysis of base-isolated RC frame structures. Earthq Eng Struct Dyn 1999;28(6):633–53. https://doi.org/10.1002/(SICI)1096-9845(199906)28:6< 633::AID-EQE832> 3.0.CO;2-3.
[10] Erduran E, Dao ND, Ryan KL. Comparative response assessment of minimally compliant low-rise conventional and base-isolated steel frames. Earthq Eng Struct Dyn 2011;40(10):1123–41. DOI: 10.1002/eqe.1078.
[11] Seranaj A, Garevski M. The required ductility reduction of soft storey buildings through application of base isolation. Res Eng Struct Mat 2018;4(1):49–60. https://doi.org/10.17515/resm2016.78ea0726.
[12] Kalfas KN, Amirabad NG, Forcellini D. The role of shear modulus on the mechanical behavior of elastomeric bearings when subjected to combined axial and shear loads. Eng Struct 2021;248:113248. https://doi.org/10.1016/j.engstruct.2021.113248.
[13] Forcellini D, Kalfas KN. Inter-story seismic isolation for high-rise buildings. Eng Struct 2023;275:115175. https://doi.org/10.1016/j.engstruct.2022.115175.
[14] Forcellini D. An expeditious framework for assessing the seismic resilience (SR) of structural configurations. Structures 2023;56:105015. https://doi.org/10.1016/j.istruc.2023.105015.
[15] Forcellini D. Assessment of geotechnical seismic isolation (GSI) as a mitigation technique for seismic hazard events. Geosciences 2020;10(6):222. https://doi.org/10.3390/geosciences10060222.
[16] Forcellini D. Seismic assessment of a benchmark base-isolated ordinary building with soil structure interaction. Bull Earthq Eng 2018;16(9):2021–42. https://doi.org/10.1007/s10518-017-0268.
[17] De Domenico D, Ricciardi G, Infanti S, Benzoni G. Frictional Heating in Double Curved Surface Sliders and Its Effects on the Hysteretic Behavior: An Experimental

Study. Frontiers in Built Environment 2019;5. https://doi.org/10.3389/fbuil.2019.00074.
[18] Almansa FL, Weng D, Li T, Alfarah B. Suitability of seismic isolation for buildings founded on soft soil. Case study of a RC building in Shanghai. Buildings 2020;10(12):241. https://doi.org/10.3390/buildings10120241.
[19] Kaatsız K, Alıcı FS, Sucuoğlu H, Tanışer S, Kale Ö. Seismic performance assessment of base isolation systems in five hospitals during the Mw7. 8 and Mw7. 6 2023 earthquakes in Southeast Turkey. 87552930241284613 Earthq Spectra 2024. https://doi.org/10.1177/87552930241284613.
[20] Massimino, M.R., Abate, G., Fiamingo, A., & Pitilakis, D. (2022, September). Seismic risk and environmentally friendly solutions: the geotechnical point of view. In International Scientific Conference Environmental Challenges in Civil Engineering (pp. 3-22). Cham: Springer International Publishing. https://doi.org/10.1007/978-3-031-26879-3_1.
[21] Abate G, Fiamingo A, Massimino MR. The role of DSSI on the seismic risk assessment of a building. In *International Scientific Conference Environmental Challenges in Civil Engineering*. Cham: Springer International Publishing; 2022. p. 48–63. ttps://doi.org/10.1007/978-3-031-26879-3_4.
[22] Tomeo R, Pitilakis D, Bilotta A, Nigro E. SSI effects on seismic demand of reinforced concrete moment resisting frames. Eng Struct 2018;173:559–72. https://doi.org/10.1016/j.engstruct.2018.06.104.
[23] de Silva F, Ceroni F, Sica S, Silvestri F. Non-linear analysis of the Carmine bell tower under seismic actions accounting for soil–foundation–structure interaction. Bull Earthq Eng 2018;16(7):2775–808. https://doi.org/10.1007/s10518-017-0298-0.
[24] Tarı U, Tüysüz O, Can Genç Ş, İmren C, Blackwell BA, Lom N, Beyhan M. The geology and morphology of the Antakya Graben between the Amik Triple Junction and the Cyprus Arc. Geodin Acta 2013;26(1-2):27–55. https://doi.org/10.1080/09853111.2013.858962.
[25] Stewart JP, Fenves GL, Seed RB. Seismic soil-structure interaction in buildings. I: Analytical methods. J Geotech Geoenviron Eng 1999;125(1):26–37. https://doi.org/10.1061/(ASCE)1090-0241(1999)125:1(26).
[26] Mekki M, Elachachi SM, Breysse D, Zoutat M. Seismic behavior of RC structures including soil-structure interaction and soil 0variability effects (Nov) Eng Struct 2016;126:15–26. https://doi.org/10.1016/j.engstruct.2016.07.034.
[27] Qu Z, Wang F, Chen X, Wang X, Zhou Z. Rapid report of seismic damage to hospitals in the 2023 Turkey earthquake sequences. Earthq Res Adv 2023;3(4):100234. https://doi.org/10.1016/j.eqrea.2023.100234.
[28] AFAD Turkish Directorate of Disaster and Emergency Management (2023) Announcements. Available at: ⟨https://www.afad.gov.tr/duyurular⟩.
[29] CEN (European Committee for Standardization). 2005. Eurocode 8: Design of structures for earthquake resistance. Part 1: General Rules, seismic actions and rules for buildings. EN 1998-1: 2005. Brussels, Belgium: CEN.
[30] Carvalho G, Bento R, Bhatt C. Nonlinear static and dynamic analyses of reinforced concrete buildings—Comparison of different modelling approaches. Earthq Struct 2013;4(5):451–70. https://doi.org/10.12989/eas.2013.4.5.451.
[31] Abdel Raheem SA, Omar M, AbdelZaher AK, Taha AM. Effects of numerical modeling simplification on seismic design of buildings. Couple Syst Mech 2018;7(6):731–53. https://doi.org/10.12989/csm.2018.7.6.731.
[32] Newmark NM. Amethodofcomputation forstructural dynamics. J Eng Mech Div 1959;85(3):67–94. https://doi.org/10.1061/JMCEA3.0000098.
[33] Mylonakis G, Gazetas G. Seismic soil-structure interaction: beneficial or detrimental? J Earthq Eng 2000;4(3):277–301. https://doi.org/10.1080/13632460009350372.
[34] NIST. 2012. Soil-structure interaction for building structures. Gaithersburg, MD: NIST.
[35] Pais A, Kausel E. Approximate formulas for dynamic stiff nesses of rigid foundations. Soil Dyn Earthq Eng 1998;7(4):213–27. https://doi.org/10.1016/S0267-7261(88)80005-8.
[36] Tsang HH, Pitilakis K. Mechanism of geotechnical seismic isolation system: analytical modeling. Soil Dyn Earthq Eng 2019;122(Jul):171–84. https://doi.org/10.1016/j.soildyn.2019.03.037.
[37] Anand V, Kumar SS. Seismic soil-structure interaction: A state-of-the-art review. In Vol. 16 of Structures. Amsterdam, Netherlands: Elsevier; 2018. p. 317–26. https://doi.org/10.1016/j.istruc.2018.10.009.
[38] Elwardany H, Seleemah A, Jankowski R, El-Khoriby S. Influence of soil–structure interaction on seismic pounding between steel frame buildings considering the effect of infill panels. Bull Earthq Eng 2019;17(11):6165–202. https://doi.org/10.1007/s10518-019-00713-1.
[39] Oz I. Seismic pounding effects of typical midrise reinforced concrete structures subjected to soil–structure interaction effects. J Struct Eng 2025;151(2). https://doi.org/10.1061/JSENDH.STENG-13659.
[40] Forcellini D. Analytical fragility curves of shallow-founded structures subjected to Soil-Structure Interaction (SSI) effects. Soil Dyn Earthq Eng 2021;141:106487. https://doi.org/10.1016/j.soildyn.2020.106487.
[41] Forcellini D. A 3-DOF system for preliminary assessments of the interaction between base isolation (BI) technique and soil structure interaction (SSI) effects for low-rise buildings. Structures 2024;59:105803. https://doi.org/10.1016/j.istruc.2023.105803.
[42] PEER (Pacific Earthquake Engineering Research Center). 2021. “Strong ground motion database.” Accessed January 21, 2021. https://ngawest2.berkeley.edu/.
[43] Castaldo P, Palazzo B, Della Vecchia P. Seismic reliability of base-isolated structures with friction pendulum bearings. Eng Struct 2015;95:80–93. https://doi.org/10.1016/j.engstruct.2015.03.053.